



A Comprehensive Comparison and Analysis of Several Intensity Modulations Based on the Underwater Photon-Counting Communication System

Xiaotian Han^{1,2}, Peng Li¹, Chang Chang¹, Duorui Gao¹, Dongquan Zhang¹, Peixuan Liao¹, Wei Wang^{1*} and Xiaoping Xie^{1,2*}

¹State Key Laboratory of Transient Optics and Photonics, Xi'an Institute of Optics and Precision Mechanics, Chinese Academy of Science, Xi'an, China, ²School of Future Technology, University of Chinese Academy of Science, Beijing, China

OPEN ACCESS

Edited by:

Yufei Ma,
Harbin Institute of Technology, China

Reviewed by:

Heping Zeng,
East China Normal University, China
Shuangyi Yan,
University of Bristol, United Kingdom

*Correspondence:

Wei Wang
wangwei2012@opt.ac.cn
Xiaoping Xie
xyp@opt.ac.cn

Specialty section:

This article was submitted to
Optics and Photonics,
a section of the journal
Frontiers in Physics

Received: 15 November 2021

Accepted: 14 December 2021

Published: 31 January 2022

Citation:

Han X, Li P, Chang C, Gao D, Zhang D,
Liao P, Wang W and Xie X (2022) A
Comprehensive Comparison and
Analysis of Several Intensity
Modulations Based on the Underwater
Photon-Counting
Communication System.
Front. Phys. 9:815343.
doi: 10.3389/fphy.2021.815343

Underwater wireless optical communication is facing absorption, scattering problems, which, in principle, can be greatly resolved by underwater photon-counting communication (UPCC) technology that exhibits high-sensitivity communication characteristics in long-range underwater wireless optical communication. Recent studies on UPCC are mainly focused on a single intensity modulation such as on-off keying (OOK) and pulse position modulation (PPM) technologies, and the comprehensive analysis of communication performance combining OOK modulation and digital pulse modulations remains a lack. To this, by using a UPCC system based on a single-photon avalanche diode, we reveal the communication performances of OOK, PPM, differential pulse interval modulation (DPIM), differential pulse position modulation (DPPM), and dual-header pulse interval modulation, and find that (1) the PPM has the longest transmission distance at the same bit error ratio when $M > 2$, but the lowest communication rate under identical modulation bandwidth and average transmit power; and (2) the DPPM and DPIM perform the optimum communication performance at the fixed communication rate when $M = 8$. We thus conclude that the DPPM and DPIM have advantages of low modulation bandwidth and long time slot time compared with PPM, indicating the significance of reducing the difficulty of signal synchronization and the complexity of the underwater photon-counting system accordingly.

Keywords: underwater wireless optical communication (UWOC), intensity modulation (IM), direct detection (DD), digital pulse modulation, photon counting, channel model

INTRODUCTION

Lasers, since their invention, have been widely used in the fields of sensing [1], communication [2], and measurement [3] because of their special characteristics such as high directionality, high brightness, monochromaticity, and good coherence. Especially in recent years, with the increase in comprehensive ocean observations in scientific, industrial, and military activities, building efficient, flexible, and reliable marine environmental sensing networks is becoming urgent and important [4].

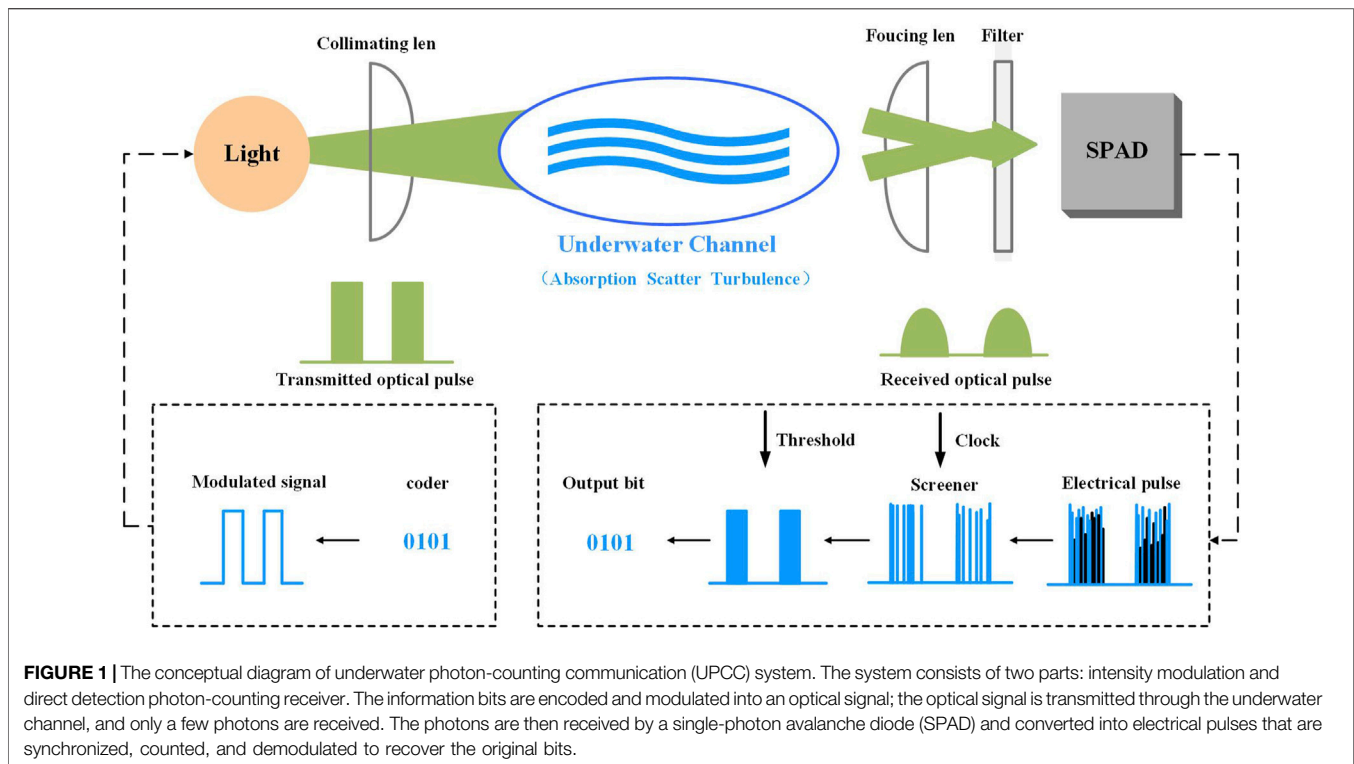
In fact, any sensors need to be linked to each other in some way of communication, so there is great interest around how to communicate between marine mobile sensing devices in a high-speed and reliable way [5]. For underwater wireless communication, the existing communication methods mainly include hydroacoustic communication, microwave communication, optical communication, and so on [6]. Underwater wireless optical communication (UWOC) is a technology that uses the blue/green light in the visible spectrum as the information carrier for signal transmission in water [7] and has the advantages of high data transmission rate, low latency, high bandwidth, low power consumption, and so on, compared with the hydroacoustic communication and microwave communication [8]. However, achieving long-range, high-speed underwater wireless optical transmission still faces challenges due to the existence of severe water attenuation and the bandwidth limitations of blue-green wavelength devices [9]. This makes high-speed signal modulation and demodulation techniques and high-sensitivity reception techniques an important research topic in the field of UWOC. Currently, the main modulation methods include intensity modulation (IM) [10], nonlinear frequency conversion [11], subcarrier modulation [12], higher-order modulation, signal multiplexing [13], and so on. The nonlinear frequency conversion technique can generate high-speed blue-green light signals with the help of mature 1,064-nm high-power devices, but the coherence of the optical signal is demanded in the frequency doubling process that high-energy consumption is needed because of the low electro-optical conversion efficiency. Although subcarrier modulation, higher-order modulation, and signal multiplexing techniques can significantly increase the data transmission rate of the system, they require high water quality and system stability and are applicable only to the laboratory technology research stage; the adaptability of these modulation techniques to the underwater channel needs further verification. In practical engineering applications, the IM techniques represented by on-off keying (OOK) are still the preferred choice. However, the high requirements for transmitting optical power for long-range underwater communications make OOK modulation unsuitable for applications on energy-limited underwater platforms. Thus, it is necessary to study the channel suitability of IM techniques with high-power utilization efficiency for underwater channels.

High-energy utilization modulation technologies represented by pulse position modulation (PPM) and high-sensitivity reception technology represented by photon-counting have become hot topics to improve power efficiency and achieve long-distance transmission. Theoretically, Hiskett et al. [14] first proposed to apply the photon-counting reception technology into underwater communication. Mao et al. [15] formulated the output characteristics of the single-photon avalanche diode (SPAD) as an ideal Poisson model and investigated the communication performance of long-range underwater photon-counting communication (UPCC) system applied with OOK modulation. Wang [16] established a long-distance underwater visible light communication system with a two-term exponential channel model and a SPAD receiver, and the arrived link distance in pure seawater can be extended to

500 m by proposing the SPAD detection algorithm. Sarbazi et al. [17] investigated the bit error performance of the receiver based on SPAD array with OOK modulation in various array sizes, dead time, and background count rate. Experimentally, Rao et al. [18] demonstrated a multirate UPCC system at data rates up to 10.416 Mbps over a 9.1-m tap water channel. Hu et al. [19] achieved a PMT-based UPCC system using a 256-PPM; the length of channel and communication sensitivity are 120 m and 3.32 bits/photon in Jerlov II water. Chen et al. [20] used a 520-nm laser diode modulation to generate the OOK signal, whereas a high-sensitivity silicon photomultiplier was used at the receiver side to achieve an attenuation length of more than 14 at a communication rate of 20 Mbps.

By and large, in the reported research articles about UPCC systems, the research and analysis are based on a single IM such as OOK or PPM. It is well known that the OOK is one of the simplest IM techniques with high bandwidth utilization, but low power utilization makes the signal transmission distance limited. For PPM, the high-power utilization makes the signal transmission distance much higher, but low bandwidth utilization leads to a short bit duration, making it difficult for signal synchronization. Furthermore, digital pulse modulation techniques including differential pulse position modulation (DPPM), differential pulse interval modulation (DPIM), and dual-header pulse interval modulation (DH-PIM), combining both bandwidth utilization and power utilization, are expected to be a good alternative modulation technique for UPCC system in some application scenarios. Therefore, a comparative analysis of the communication performance of OOK modulation and various digital pulse modulations is not only important for optimizing the performance of the UPCC system, but also an important guide for the design of communication systems. Of course, as far as modulations are concerned, similar comparisons have been made by numerous researchers, but mostly based on positive-intrinsic-negative (PIN) and avalanche photodiode (APD) receivers. However, single-photon detector-based receivers differ from conventional PIN and APD-based receivers in terms of the statistical model of the signal output [21]. Therefore, it is significant to compare the performance of multiple IM schemes based on the photon counting receiver model.

In this article, an underwater photon counting system is built based on IM and direct detection (IM/DD) photon counting reception technique. First, this article introduces the bit-symbol mapping principles of OOK, PPM, DPPM, DPIM, and DH-PIM; the seawater channel model; the statistical model of the output of the SPAD under the influence of dead time; and the minimum error judgment criterion to obtain the expressions for the bit error ratio (BER) calculation. Second, the performance parameters of a commonly used UWOC system and a commercially available SPAD detector are selected to analyze and compare the communication performance of different IM methods in a pure seawater channel. For one thing, the article compares the variation of BER with a transmission distance of communication system for different modulation schemes when modulation bandwidth is fixed. For another thing, the same analysis is done under a fixed communication rate. Finally, the simulation results are shown and discussed.



UPCC SYSTEM MODELING

The system architecture of UPCC, as shown in **Figure 1**, is composed of two parts: IM and DD photon-counting receiver. As demonstrated in **Figure 1**, the source bit is encoded and modulated into the optical carrier; the optical signal is transmitted through the underwater channel and degraded by the absorption, scattering, and turbulence effects of the medium. At the receiver, the photon-counting receiver that uses a SPAD working in counting mode is used to receive and process single-photon signals. When the receiver works, the SPAD detects the weak photon signal to generate a single electrical pulse signal, and a large number of noise pulses are introduced due to SPAD dark counts and background noise. For these reasons, a screener is used to extract useful information by rejecting noisy count pulses regarding the synchronous clock. Finally, the count module counts the signal pulses within a certain period, and counted signal pulses are used to restore the initial code stream signal by comparing it with the threshold value. In addition, to increase the reliability of data transmission, communication systems often use channel coding and equalization, and so on. It should be noted that it is assumed that the UPCC system has been clock synchronized at both the transceiver side in this study.

The Modulation Schemes for OOK and Digital Pulse Modulations

In the UPCC system with IM/DD, OOK and PPM are the commonly used IM schemes. Compared with OOK modulation, PPM has higher power utilization efficiency but

lower bandwidth utilization [22], which is often used in photon-counting communication systems to improve sensitivity. To optimize the bandwidth utilization of PPM, many digital pulse modulation schemes have been developed, such as DPPM, DPIM, DPIM, and DH-PIM. OOK modulation uses one optical pulse to represent a 1-bit signal, whereas digital pulse modulations decompose a signal symbol into multiple time slots; the position of the optical pulse within a symbol is used to represent multiple bits, with the remaining slots being empty. DPPM removes the redundant time slots that exist in PPM. For DPIM, each symbol begins with a slot-duration pulse, followed by a series of empty data slots, the number of which depends on the decimal value of the encoded M -bit data stream. To mitigate intersymbol interference degradation of the signal, a guard slot consisting of one or more empty slots is added after the pulse. Compared with PPM, DPPM, and DPIM, DH-PIM not only removes the redundant time slots that follow the pulse in the PPM and but also reduces the average symbol length compared with DPIM. The time-domain waveforms of OOK and several digital pulse modulation schemes are shown in **Figure 2** [23]. As shown in the figure, to have the same data throughout as OOK, the slot duration time T_s of digital pulse modulation is shorter than the OOK bit duration time T_b .

For IMs, the digital signal is loaded into the carrier wave by modulating the intensity and position of a light wave. The biggest difference between these modulations is the number of slots in a single symbol, which influences directly the transmit optical power per ON slot. The more slots, the higher transmit optical power per ON slot when the average optical transmit power keeps fixed; the relation between the mean transmit power

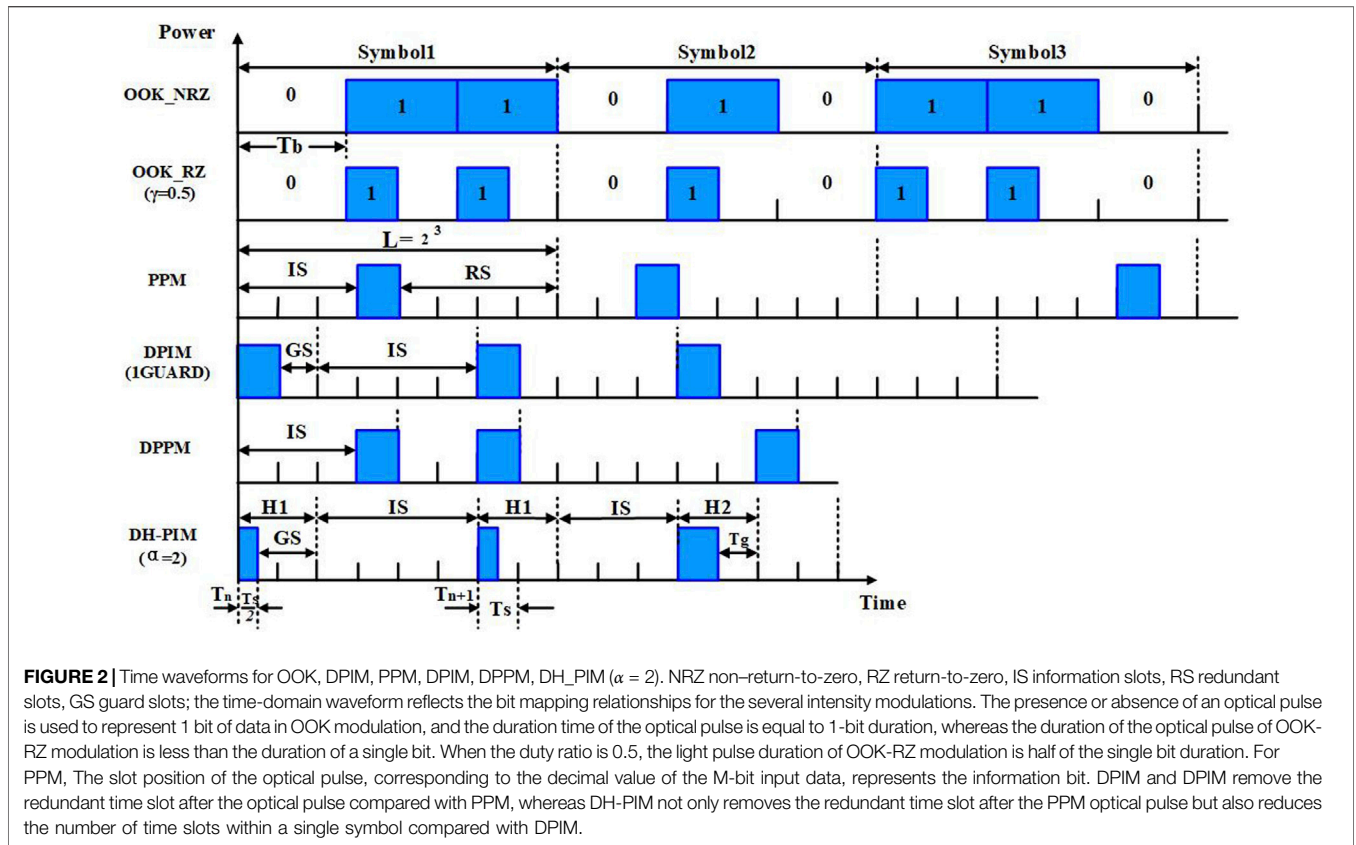


TABLE 1 | The modulation orders and the communication rates for different modulation schemes under a given B and M [23].

Modulation schemes	Modulation order (L or \bar{L})	Rates (R_b)
PPM	2^M	$MB/2^M$
DPIM(1GUARD)	$(2^M + 3)/2$	$2MB/(2^M + 3)$
DPPM	$(2^M + 1)/2$	$2MB/(2^M + 1)$
DH-PIM	$(2^{M-1} + 2\alpha + 1)/2$	$2MB/(2^{M-1} + 2\alpha + 1)$

per symbol and optical power per ON slot can be expressed as $P_{ON} = LP_{average}$, where $P_{average}$ is the average optical of a symbol, and L is the length of a single symbol or usually named the modulation order. For OOK_NRZ and OOK_RZ, L is equal to 2 and 4, respectively. For the PPM, $L = 2^M$ [24]. For DPPM, DPIM, and DH-PIM, different symbols have different numbers of time slots, so the symbol length is represented by the average symbol length, and the average symbol length \bar{L} can be found in [23]. The modulation orders and the communication rates for different modulation schemes under a given modulation bandwidth ($B = 1/T_s$) are listed in **Table 1**.

Underwater Channel Model

The absorption and scattering of the light by the seawater will cause the attenuation of the energy of the optical signal, especially when the turbidity of seawater is high; the signal quality will also

deteriorate. The extinction coefficient $c(\lambda)$ of seawater on light, which is determined by the absorption coefficient $a(\lambda)$ and scattering coefficient $b(\lambda)$ of seawater, can be expressed by the formula [25]:

$$c(\lambda) = a(\lambda) + b(\lambda) \tag{1}$$

In the formula, the units of the three parameters are m^{-1} . The energy loss factor $L(\lambda, z)$, decided by the light beam transmission distance z (m) and the wavelength λ (nm) of light, can be given by the following equation [26].

$$L(\lambda, z) = e^{-c(\lambda)z} \tag{2}$$

The coefficients $a(\lambda)$, $b(\lambda)$, and $c(\lambda)$ for Petzold seawater types are presented in **Table 2** at the wavelength of 532 nm, which are taken from [27].

Many channel models of UWOC can be obtained from [25, 28–31]. When an optical beam is transmitting in the pure seawater and clear seawater, the temporal spread of the optical pulse can be neglected. Geometric Beer’s Law (GBL) can be applied to these two water types to calculate the geometric attenuation since the beam spreading and alignment error [32]. In this article, we consider the line-of-sight communication link model. In this scenario, the light beam is directed from a transmitter into a receiver; both telescope gain and loss are taken into account, the optical signal reaching the receiver is obtained by [25]:

TABLE 2 | Absorption, scattering, and extinction coefficient for the Pure seawater and three Petzold water types.

Water type	Pure seawater	Clear seawater	Coastal seawater	Harbor seater
a (m ⁻¹)	0.0405	0.114	0.179	0.266
b (m ⁻¹)	0.0025	0.037	0.219	1.824
c (m ⁻¹)	0.043	0.151	0.298	2.190

$$P_R = \begin{cases} P_{ON}\eta_T\eta_R L\left(\lambda, \frac{d}{\cos\theta}\right) \frac{A_{Rec} \cos\theta}{2\pi d^2 (1 - \cos\theta_0)} & \theta_0 \\ P_{ON}\eta_T\eta_R L\left(\lambda, \frac{d}{\cos\theta}\right) \frac{A_{Rec} \cos\theta}{\pi (d \tan\theta_0)^2} & \theta_0 \ll \pi/20 \end{cases} \quad (3)$$

where P_{ON} is the transmitted-light power per slot, η_T is the optical efficiency of the transmitter, η_R is the efficiency of the receiver, d is the perpendicular distance between the transmitter and receiver plane, and θ is the angle between the perpendicular to the receiver plane and the transmitter-receiver trajectory, also known as the angle of inclination between transmitter and receiver. A_{Rec} is the receiver aperture area, and θ_0 is the optical beam divergence angle (half-angle transmit beam width) [25].

Underwater Turbulence Model

In the practical application of UWOC, considering aperture average effect, received optical power under the influence of underwater optical turbulence can be represented by log-normal distribution from weak to strong turbulence condition, which has been validated by a large number of field experiments. The probability density function (PDF) $f(I)$ for the underwater channel can be expressed by the log-normal function [33]:

$$f(I) = \frac{1}{P\sigma\sqrt{2\pi}} \exp\left(-\frac{(\ln(I/I_0) + \sigma^2/2)^2}{2\sigma^2}\right) \quad (4)$$

where I_0 is the mean received light energy in the time interval $[0, T_s]$. For plane-wave, the scintillation index (S.I), σ , can be expressed as [34]:

$$\sigma^2 = \exp\left(\frac{0.49\sigma_r^2}{(1 + 1.11\sigma_r^{12/5})^{7/6}} + \frac{0.51\sigma_r^2}{(1 + 0.69\sigma_r^{12/5})^{5/6}}\right) - 1 \quad (5)$$

where σ_r^2 is the Rytov variance; the classical Kolmogorov spectrum model can be given [35]:

$$\sigma_r^2 = 44.76\epsilon^{2/3} \left(\frac{\partial T}{\partial z}\right)^2 \left(\frac{2\pi}{\lambda_{light}}\right)^{7/6} z^{11/6} N^{-1} \quad (6)$$

where ϵ is the turbulence kinetic energy dissipation rate, $\partial T/\partial z$ is the temperature gradient, λ_{light} is the optical wavelength, z is the transmitting distance of the light beam, and N represents the buoyancy frequency.

SPAD Photon-Counting Receiver Model

When the UWOC works, assume the average signal photon rate reaching the front end of the detector is the constant λ_s , the average background photon-counting rate is the constant λ_b , and the dark count rate of SPAD is the constant λ_d . Of course, the

other parameters including afterpulsing and timing-jitter, crosstalk, and fill-factor should also be considered, but in this article, we neglect these influences. Thus, the SPAD's photoelectron count model can be given:

$$\lambda = \begin{cases} \eta\lambda_s + \eta\lambda_b + \lambda_d & \text{signal} \\ \eta\lambda_b + \lambda_d & \text{no - signal} \end{cases} \quad (7)$$

where η is the photon detection efficiency of SPAD, the average photon arrival rate λ_s , and λ_b is related to the received optical power P_R of signal and background P_b ; the relational expression is given as:

$$\lambda_s = \frac{\eta P_R}{h\nu} \quad (8)$$

$$\lambda_b = \frac{\eta P_b}{h\nu} \quad (9)$$

where h is the Planck constant, and ν is the frequency of the single photon.

We assume the sampling rate of SPAD is very high compared with the dead time so that the counting losses due to finite sampling rate can be negligible. If the dead time of SPAD is the constant τ , the maximum number of photons recorded by SPAD during the slot interval time $[0, T_s]$ can be expressed as $k_{max} = [T_s/\tau] + 1$, where $[x]$ is the maximum that is smaller than x . The PDF of counting k photons in a timing period $[0, T_s]$ is given [36]:

$$p(k, \lambda, T_s) = \begin{cases} \sum_{i=0}^k \frac{\lambda^i (T_s - (k+1)\tau)^i}{i!} \exp(-\lambda(T_s - (k+1)\tau)) & k < k_{max} \\ -\sum_{i=0}^{k-1} \frac{\lambda^i (T_s - k\tau)^i}{i!} \exp(-\lambda(T_s - k\tau)), & \\ 0, & k \geq k_{max} \end{cases} \quad (10)$$

Bit Error Ratio Calculation

For OOK modulation, based on the principle of threshold test, the bit error ratio (BER) can be given as [37]:

$$P_{OOK} = \frac{1}{2} - \frac{1}{2} \sum_{k=0}^{k_{th}} \left[\int_0^\infty p(k, \lambda_{sn}, T_s) f(I) dI - p(k, \lambda_n, T_s) \right] \quad (11)$$

where k_{th} is the optimum decision threshold of the number of photons in the interval time $[0, T_s]$, which can be obtained by the following decision principle of the threshold.

For PPM, DPIM, DMMP, and DH-PIM symbol, the symbol error ratio (SER) for a continuous output L -order digital pulse modulation signal is [38] :

$$P_{SER} = 1 - \left[1 - \frac{1}{L} \sum_{k=0}^{k_{th}} \int_0^{\infty} p(m, \lambda_{sn}, T_s) f(I) dI - \frac{L-1}{L} \sum_{k=k_{th}}^{\infty} p(k, \lambda_n, T_s) \right]^L \tag{12}$$

The SER can be converted into BER by:

$$P_{BER} = \frac{LP_{SER}}{2(L-1)}$$

Based on the principle of minimum error probability [39], by solving the following Eq. 13, we can get the optimum threshold k_{th} .

$$\frac{\int_0^{\infty} p(k, \lambda_{sn}, T_s) f(I) dI}{p(k, \lambda_n, T_s)} = \frac{P(0)}{P(1)} \tag{13}$$

where $P(0)$ and $P(1)$ are a prior probability of time slot detection.

NUMERICAL RESULTS AND DISCUSSION

In this research, with the assumption of negligible delay spread, based on the GBL model and SPAD photon-counting receiver model, we establish the relationship between the BER and attenuation length on the underwater wireless UPCC system in the pure seawater. The effect of M on various IM schemes is also investigated. The parameters of the UWOC system are listed in Table 3. In the following discussion, the specifications of the SPCM20A from Thorlabs [40] have been applied to this simulation. The values of other parameters characterize the classical channel of the UWOC system. According to [41], the attenuation length, which is defined as the multiple of the transmission distance and attenuation coefficient, is used to represent the link transmission distance to remove the ambiguity of distance and various water conditions. In addition, with the assumption of negligible slot time delay spread, the degradation of signal bandwidth and the intersymbol caused by channel transmission can be ignored. Therefore, the mathematical relationship between data rate and modulation bandwidth in Table 1 [23] can be used in this article.

On the one hand, BERs for OOK, PPM, DPIM, DPPM, and DH-PIM as the function of attenuation length when $T_s = 15\tau$ (modulation bandwidth $B = 1.9$ Mbps) are given in Figure 3. The forward-error-correction (FEC) limit of 3.8×10^{-3} , a commonly used BER at some of the reported UWOC systems [42–44], and some FEC codes providing reliable communication with an overhead of approximately 7% [45], is regarded as a criterion for evaluation in this article. As shown in Figure 3, BERs of all modulation schemes rise with the increment of attenuation length. At the FEC limit, the OOK system can arrive the maximum attenuation length for $M = 2$, and the attenuation length that the DH_PIM system can achieve its minimum. For the fixed modulation bandwidth and average transmit power, to achieve the same BER, the UPCC system for all digital pulse modulation schemes transmits over a shorter distance than the

TABLE 3 | Parameters of UPCC system.

Parameter	Symbol	Value
The wavelength of lighter (nm)	λ	532
Extinction coefficient (m^{-1})	c	0.045
Divergence angle (rad)	λ_0	0.1745
Average transmit power (W)	P_T	1.0
Transmitter inclination angle (rad)	θ	0
Photon efficiency of the transmitter	η_T	0.9
The optical efficiency of the receiver	η_R	0.9
Receiver aperture (mm)	D	350
Photon detection efficiency@532 nm	η	35%
Deadtime (ns)	τ	35
Dark count rate (counts/sec)	λ_d	60
Background photon count (counts/slot)	λ_b	0.01
Average turbulence kinetic energy (m^2s^{-3})	ϵ	3×10^{-10}
temperature gradient ($^{\circ}C m^{-1}$)	$\partial T/\partial z$	7.94×10^{-6}
Average buoyancy frequency(s^{-1})	$\langle N \rangle$	2.9×10^{-4}

OOK_RZ modulation system when $M = 2$. The longer the transmission distance, the higher the power utilization is. Thus, the DPIM with a guard slot has higher power utilization than DPPM, and the power utilization of PPM is the highest. As bit resolution improves, when $M = 4, 6, 8$, the power utilizations of DH-PIM ($\alpha \leq 4$), DPPM, DPIM (1GUARD), and PPM have higher power utilization than OOK modulation, and the power utilization of DPPM and DPIM(1GUARD) tends to keep consistent. When the modulation bandwidth and average transmit power are certain, it should be noted that the communication distance that can be achieved by OOK modulation at a given BER does not change with M .

DH-PIM is one of the digital pulse modulations. Compared with PPM and PIM, DH_PIM not only removes the redundant time slots that follow the pulse in the PPM but also reduces the average symbol length compared with PIM [46]. In DH-PIM, the n th symbol starts with a header duration and follows with a sequence of d_n empty slots, the header duration consists of a header pulse H_n and a guard band G_n , and the value of d_n is the decimal value of modulated binary codeword within a symbol. If the value of $d_n \in \{0, 1, \dots, 2^{M-1}\}$, H_1 will be as header pulse; otherwise, the header pulse will be H_1 . The duration time of the header H_1 and H_2 is $0.5\alpha T_s$ and αT_s , respectively; each header pulse is followed by a guard band $G_n \in \{(0.5\alpha + 1)T_s, T_s\}$; the number of empty slots is equal to the decimal value of modulated binary codeword and the decimal value of complement of the modulated binary word. In this modulation, the header pulse plays dual roles of symbol initial and time reference for preceding and succeeding symbol. For the value, α , which is an adjustment factor, the average symbol length \bar{L} of DH_PIM will be changed by adjusting α . When α is reduced, the reduction of average symbol length improves transmission throughput. By analysis, we can conclude that with increasing the α , the BER becomes bigger gradually when the system transmits the same attenuation length, or when BER is a constant, the smaller the adjustment factor α , the bigger the attenuation length.

As the results of the above analysis, increasing the value of the M for the same modulation bandwidth significantly improves the power utilization of the digital pulse

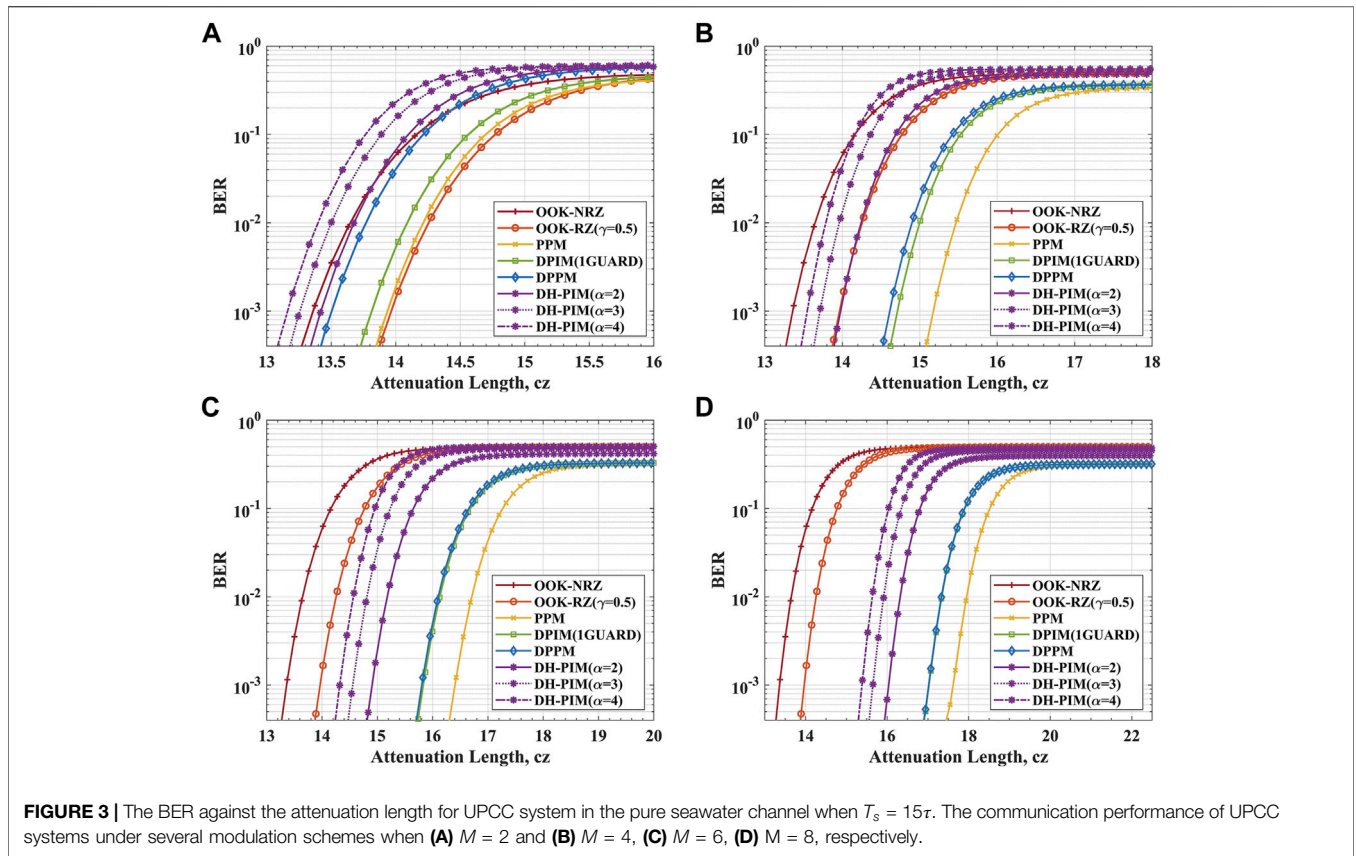


FIGURE 3 | The BER against the attenuation length for UPCC system in the pure seawater channel when $T_s = 15\tau$. The communication performance of UPCC systems under several modulation schemes when (A) $M = 2$ and (B) $M = 4$, (C) $M = 6$, (D) $M = 8$, respectively.

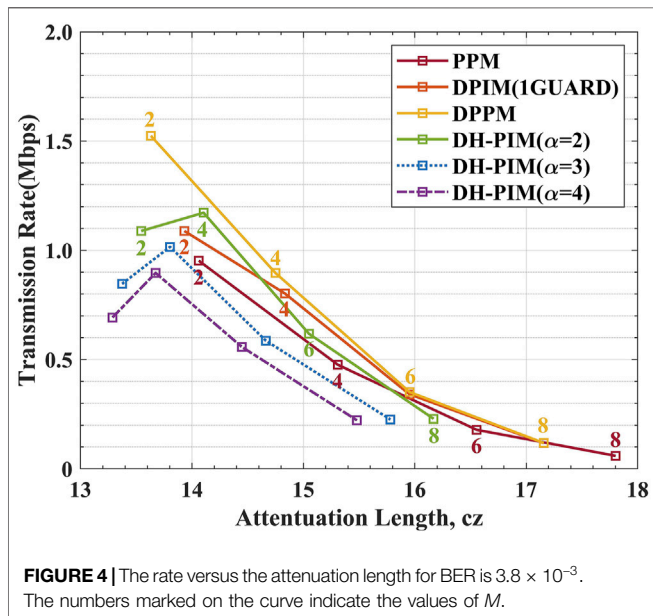
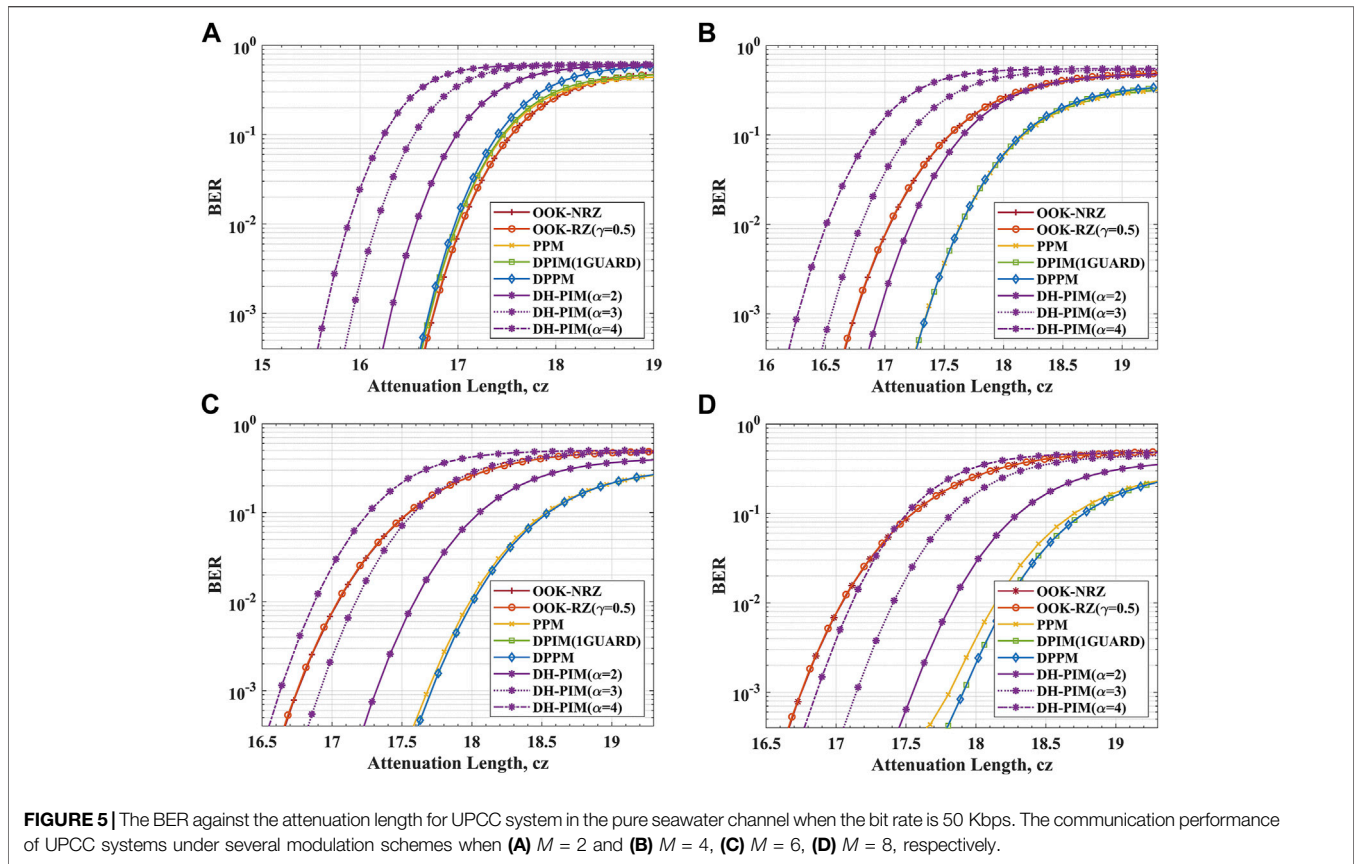


FIGURE 4 | The rate versus the attenuation length for BER is 3.8×10^{-3} . The numbers marked on the curve indicate the values of M .

modulation so that the attenuation length of the system increases. However, M is related to the bandwidth utilization, which decides the transmission rate of a communication system. The higher transmission rate means the higher bandwidth utilization for the same M .

We limit the BER simulation results to below the FEC limit; the transmission rates and attenuation lengths of a system for DH-PIM, PPM, DPPM, and DPIM under the different M are shown in Figure 4. This figure clearly shows the trade-off between transmission rate and attenuation length. For PPM, DPIM, and DPPM systems, the attenuation length increases with M , but the transmission rate decreases accordingly. This is because for digital pulse modulation schemes, when the modulation bandwidth is fixed, the power utilization is proportional to the value of M , and the bandwidth utilization is inversely proportional to M . For DPIM with a guard slot, the transmission rate and attenuation length of the system are almost the same for $M = 6$ and $M = 8$. Comparing the performance of DPIM with a guard slot and PPM, the system for the PPM scheme can achieve a longer transmission length, but the transmission rate is lower than the DPIM system at a certain value of M . For DH-PIM, the bandwidth utilization efficiency is the highest of all digital pulse modulations, and it is evident that there is the highest point of transmission rate for DH-PIM when $M = 4$.

On the other hand, to do a fair comparison between the different IM schemes, the communication performance of the UPCC system under the various IM schemes is compared when the data rate and average transmit optical power are fixed. As shown in Figure 5, setting the bit rate to 50 Kbps, the value of M is 2, 4, 6, 8 in sequence. When $M = 2$ and BER is the



FEC limit, the minimum attenuation length that DH-PIM ($\alpha = 4$) can transmit is approximately 15.74 and the maximum attenuation length that OOK-RZ can transmit is approximately 16.90. Similarly, when $M = 4$, the attenuation lengths of DH-PIM ($\alpha = 4$) and OOK-RZ are 16.38 and 16.90, respectively. When M is 6 and 8 separately, the attenuation lengths of DH-PIM ($\alpha = 4$) and OOK (OOK-NRZ and OOK-RZ) can arrive at 16.73 and 16.90, and 16.99 and 16.90. We can conclude that the performance of the OOK keeps constant, but the other system performances do not improve much with the increase in M . For digital pulse modulation schemes, the power utilization is proportional to the value of M , and the bandwidth utilization is inversely proportional to M . The power utilization is improved, and the bandwidth utilization is decreased with the increase in M . When the transmission rate keeps fixed, an increasing M affects both the bandwidth utilization and the power utilization of the system, which makes the performance of the system with digital pulse modulations not improve much. But, for OOK, the power utilization and the bandwidth utilization keep constant with the increase in M ; the performances of the OOK as M increases have no changes. Compared with digital pulse modulation schemes, OOK has poor power utilization efficiency, but good bandwidth utilization efficiency compensates for this disadvantage. Therefore, when $M = 2$, the performance of the UPCC system with OOK is much better than the other systems in

the overall comparison. As M increases, digital pulse modulations can transmit a longer attenuation length than OOK modulation. Except for DH-PIM, the digital pulse modulations can transmit a longer attenuation length than OOK modulation for $M > 2$. Various modulation schemes, including DPIM (1GUARD), DPPM, and PPM, tend to transmit the same distance at the same rate when $M = 4$ and $M = 6$. However, with the increase in the value of M , the DPPM and DPIM (1GUARD) display a more excellent communication performance compared with DH-PIM and PPM schemes when $M = 8$.

CONCLUSION

In this article, a UPCC system model based on IM and DD photon counting reception techniques is built. The article compares the variation of BER with a transmission distance of communication system for OOK, PPM, DPIM, DPPM, and DH-PIM under the same modulation bandwidth. From our analysis, we conclude that the PPM has the longest transmission distance at the same BER when $M > 2$, but the lowest communication rate. Transmission distance gets farther, and the communication rate gets lower as M increases. In addition, the same analysis is done under a fixed communication rate. It is concluded that the DPPM and DPIM have the optimum communication performance at

the same communication rate when $M = 8$. As the modulation bandwidth is lower and the time slot time is longer for DPPM and DPIM than PPM when the communication rate is the same, long slot time will help reduce the difficulty of signal synchronization and hence the complexity of the underwater photon counting system. The simulation and analysis in this article are based on published theoretical models, and the results concluded can be referenced for real transmission communication.

DATA AVAILABILITY STATEMENT

The original contributions presented in the study are included in the article/supplementary material, further inquiries can be directed to the corresponding authors.

REFERENCES

- Qiao S, Ma Y, He Y, Patimisco P, Sampaolo A, Spagnolo V. Ppt Level Carbon Monoxide Detection Based on Light-Induced Thermoelastic Spectroscopy Exploring Custom Quartz Tuning forks and a Mid-infrared QCL. *Opt Express* (2021) 29(16):25100–8. doi:10.1364/OE.434128
- Gao D, Xie Z, Ma R, Wang W, Bai Z, Jia S, et al. Analysis of the Current Situation and Trends in the Development of Satellite Laser Communications (Invited). *J Photon* (2021) 50(04):9–29. doi:10.3788/gzxb20215004.0406001
- Lang Z, Qiao S, He Y, Ma Y. Quartz Tuning fork-based Demodulation of an Acoustic Signal Induced by Photo-Thermo-Elastic Energy Conversion. *Photoacoustics* (2021) 22:100272. doi:10.1016/j.pacs.2021.100272
- Ali MF, Jayakody DNK, Chursin YA, Affes S, Dmitry S. Recent Advances and Future Directions on Underwater Wireless Communications. *Arch Computat Methods Eng* (2020) 27(5):1379–412. doi:10.1007/s11831-019-09354-8
- Kodama T, Arai K, Nagata K, Nakamura K, Hanawa M. Underwater Wireless Optical Access Network with OFDM/SBMA System: Concept and Demonstration. In: Proceeding of the 2019 24th OptoElectronics and Communications Conference (OECC) and 2019 International Conference on Photonics in Switching and Computing (PSC); 2019 July 7–11; Fukuoka, Japan. IEEE (2019). p. 18957302. doi:10.23919/ps.2019.8817754
- Ooi BS, Kong M, Ng TK. Underwater Wireless Optical Communications: Opportunity, Challenges and Future Prospects Commentary on “Recent Progress in and Perspectives of Underwater Wireless Optical Communication”. *Prog Quan Electronics* (2020) 73:100275. doi:10.1016/j.pquantelec.2020.100275
- Duntley SQ. Light in the Sea*. *J Opt Soc Am* (1963) 53(2):214–33. doi:10.1093/icb/26.2.38910.1364/josa.53.000214
- Sun X, Kang CH, Kong M, Alkhazragi O, Guo Y, Ouhssain M, et al. A Review on Practical Considerations and Solutions in Underwater Wireless Optical Communication. *J Lightwave Technol* (2020) 38(2):421–31. doi:10.1109/jlt.2019.2960131
- Saeed N, Celik A, Al-Naffouri TY, Alouini M-S. Underwater Optical Wireless Communications, Networking, and Localization: A Survey. *Ad Hoc Networks* (2019) 94:101935. doi:10.1016/j.adhoc.2019.101935
- Matthews W, Ahmed Z, Ali W, Collins S. A 3.45 Gigabits/s SiPM-Based OOK VLC Receiver. *IEEE Photon Technol Lett* (2021) 33(10):487–90. doi:10.1109/LPT.2021.3069802
- Hanson F, Radic S. High Bandwidth Underwater Optical Communication. *Appl Opt* (2008) 47(2):277–83. doi:10.1364/AO.47.000277
- Du J, Wang Y, Fei C, Chen R, Zhang G, Hong X, et al. Experimental Demonstration of 50-M/5-Gbps Underwater Optical Wireless Communication with Low-Complexity Chaotic Encryption. *Opt Express* (2021) 29(2):783–96. doi:10.1364/OE.416117
- Tsai W-S, Lu H-H, Wu H-W, Tu S-C, Huang Y-C, Xie J-Y, et al. 500 Gb/s PAM4 FSO-UWOC Convergent System with a R/G/B Five-Wavelength

AUTHOR CONTRIBUTIONS

XX, WW, and XH conceived the idea of the study; XH and PL analyzed the data, interpreted the results, and wrote the article; all authors discussed the results and revised the manuscript.

FUNDING

Program Name: Deep-sea Omni-directional High-speed Long-distance Optical. (Strategic Pioneer Science and Technology Special Project of Chinese Academy of Sciences(Class A))
Funder: Chinese Academy of Sciences Grant number: XDA22030203 Program Name: Ministry of Science and Technology Key R&D Program. Grant number: 2018YFC0307904.

- Polarization-Multiplexing Scheme. *IEEE Access* (2020) 8:16913–21. doi:10.1109/ACCESS.2020.2967856
- Hiskett PA, Struthers RA, Tatton R, Lamb R. A Photon-Counting Optical Communication System for Underwater Data Transfer. In: Proceeding of the Electro-Optical Remote Sensing, Photonic Technologies, and Applications VI; 2021 Nov. 19; Edinburgh, United Kingdom. Edinburgh, UK: International Society for Optics and Photonics (2012). p. 854214. doi:10.1117/12.974938
- Mao T, Wang Z, Wang Q. Receiver Design for SPAD-Based VLC Systems under Poisson-Gaussian Mixed Noise Model. *Opt Express* (2017) 25(2):799–809. doi:10.1364/OE.25.000799
- Wang C, Yu H-Y, Zhu Y-J. A Long Distance Underwater Visible Light Communication System with Single Photon Avalanche Diode. *IEEE Photon J* (2016) 8(5):1–11. doi:10.1109/JPHOT.2016.2602330
- Sarbazi E, Safari M, Haas H. The Bit Error Performance and Information Transfer Rate of SPAD Array Optical Receivers. *IEEE Trans Commun* (2020) 68(9):5689–705. doi:10.1109/TCOMM.2020.2993374
- Rao HG, DeVoe CE, Fletcher AS, Gaschits ID, Hakimi F, Hamilton SA. A Burst-Mode Photon Counting Receiver with Automatic Channel Estimation and Bit Rate Detection. In: SPIE Proceedings Free-Space Laser Communication and Atmospheric Propagation XXVIII; 2016 April 13; San Francisco, California, United States. San Francisco, CA: SPIE (2016). p. 9739. International Society for Optics and Photonics. doi:10.1117/12.2222885
- Hu S, Mi L, Zhou T, Chen W. 3588 Attenuation Lengths and 332 Bits/photon Underwater Optical Wireless Communication Based on Photon-Counting Receiver with 256-PPM. *Opt Express* (2018) 26(17):21685–99. doi:10.1364/oe.26.021685
- Chen Z, Tang X, Sun C, Li Z, Shi W, Wang H, et al. Experimental Demonstration of over 14 AL Underwater Wireless Optical Communication. *IEEE Photon Technol Lett* (2021) 33(4):173–6. doi:10.1109/LPT.2020.3048786
- Gabriel C, Khalighi M-A, Bourennane S, Léon P, Rigaud V. Investigation of Suitable Modulation Techniques for Underwater Wireless Optical Communication. In: Proceeding of the 2012 International Workshop on Optical Wireless Communications (IWOW); 2012 Oct. 22–22; Pisa, Italy. IEEE (2012). p. 113–4. doi:10.1109/IWOW.2012.6349691
- Wang X, Wang Y, Yao Z, Chen X, Zhu X, Zhang X. Timing Offset Estimation of PPM Signal for Deep Space Optical Communications. In: *Signal and Information Processing, Networking and Computers: Proceedings of the 6th International Conference on Signal and Information Processing, Networking and Computers (ICSINC)*. Xi'an China: Springer Nature (2020). p. 444–52. doi:10.1007/978-981-15-4163-6_53
- Ghassemlooy Z, Popoola W, Rajbhandari S. *Optical Wireless Communications: System and Channel Modelling with Matlab®*. New York, USA: CRC Press (2019). p. 204–309.
- Sato K, Asatani K. Speckle Noise Reduction in Fiber Optic Analog Video Transmission Using Semiconductor Laser Diodes. *IEEE Trans Commun* (1981) 29(7):1017–24. doi:10.1109/TCOM.1981.1095084

25. Gabriel C, Khalighi M, Bourennane S, Leon P, Rigaud V. Channel Modeling for Underwater Optical Communication. In: Proceeding of the 2011 IEEE GLOBECOM Workshops (GC Wkshps); 5-9 Dec. 2011; Houston, Tx USA. IEEE (2011). p. 6162571. doi:10.1109/GLOCOMW.2011.6162571
26. Arnon S, Kedar D. Non-line-of-sight Underwater Optical Wireless Communication Network. *J Opt Soc Am A* (2009) 26(3):530-9. doi:10.1364/JOSAA.26.000530
27. Cochenour BM, Mullen LJ, Laux AE. Characterization of the Beam-Spread Function for Underwater Wireless Optical Communications Links. *IEEE J Oceanic Eng* (2008) 33(4):513-21. doi:10.1109/JOE.2008.2005341
28. Tang S, Dong Y, Zhang X. Impulse Response Modeling for Underwater Wireless Optical Communication Links. *IEEE Trans Commun* (2014) 62(1):226-34. doi:10.1109/TCOMM.2013.120713.130199
29. Akhouni F, Salehi JA, Tashakori A. Cellular Underwater Wireless Optical CDMA Network: Performance Analysis and Implementation Concepts. *IEEE Trans Commun* (2015) 63:882-91. doi:10.1109/TCOMM.2015.2400441
30. Zhang H, Dong Y. Impulse Response Modeling for General Underwater Wireless Optical MIMO Links. *IEEE Commun Mag* (2016) 54:56-61. doi:10.1109/MCOM.2016.7402261
31. Li Y, Leeson MS, Li X. Impulse Response Modeling for Underwater Optical Wireless Channels. *Appl Opt* (2018) 57(17):4815-23. doi:10.1364/AO.57.004815
32. Huang J, Wen G, Dai J, Zhang L, Wang J. Channel Model and Performance Analysis of Long-Range Deep Sea Wireless Photon-Counting Communication. *Opt Commun* (2020) 473:125989. doi:10.1016/j.optcom.2020.125989
33. Andrews LC, Phillips RL, Hopen CY. *Laser Beam Scintillation with Applications*. Bellingham, Washington USA: SPIE press (2001). p. 112-5.
34. Cheng X, Qu F, Yang L. Single Carrier FDMA over Underwater Acoustic Channels. In: Proceeding of the 2011 6th International ICST Conference on Communications and Networking in China (CHINACOM); 17-19 Aug. 2011; Harbin. IEEE (2011). p. 6158311.
35. Weng Y, Guo Y, Alkhazragi O, Ng TK, Guo J-H, Ooi BS. Impact of Turbulent-Flow-Induced Scintillation on Deep-Ocean Wireless Optical Communication. *J Lightwave Technol* (2019) 37(19):5083-90. doi:10.1109/LT.2019.2928465
36. Sarbazi E, Safari M, Haas H. Statistical Modeling of Single-Photon Avalanche Diode Receivers for Optical Wireless Communications. *IEEE Trans Commun* (2018) 66(9):4043-58. doi:10.1109/TCOMM.2018.2822815
37. Popoola W, Ghassemlooy Z, Awan MS, Leitgeb E. *Atmospheric Channel Effects on Terrestrial Free Space Optical Communication Links 3rd International Conference on Computers and Artificial Intelligence (ECAI 2009)*. Pites ti: Citeseer (2009).
38. Hemmati H. *Deep Space Optical Communications*. California: John Wiley & Sons (2006). p. 253-5.
39. Kay SM. *Fundamentals of Statistical Signal Processing. Detection Theory, Volume II*. New York: Prentice Hall PTR (1998). p. 435-7.
40. Thorlabs. *V21 Catalog* (2011). Available at: https://www.thorlabs.com/NewGroupPage9_PF.cfm?ObjectGr_oup_ID=5255 (Accessed September 15, 2021).
41. Zhang L, Tang X, Sun C, Chen Z, Li Z, Wang H, et al. Over 10 Attenuation Length Gigabits Per Second Underwater Wireless Optical Communication Using a Silicon Photomultiplier (SiPM) Based Receiver. *Opt Express* (2020) 28(17):24968-80. doi:10.1364/OE.397942
42. Wang J, Lu C, Li S, Xu Z. 100 M/500 Mbps Underwater Optical Wireless Communication Using an NRZ-OOK Modulated 520 Nm Laser Diode. *Opt Express* (2019) 27(9):12171-81. doi:10.1364/OE.27.012171
43. Tang X, Kumar R, Sun C, Zhang L, Chen Z, Jiang R, et al. Towards Underwater Coherent Optical Wireless Communications Using a Simplified Detection Scheme. *Opt Express* (2021) 29(13):19340-51. doi:10.1364/OE.426820
44. Fei C, Hong X, Zhang G, Du J, Gong Y, Evans J, et al. 166 Gbps Data Rate for Underwater Wireless Optical Transmission with Single Laser Diode Achieved with Discrete Multi-Tone and post Nonlinear Equalization. *Opt Express* (2018) 26(26):34060-9. doi:10.1364/OE.26.034060
45. ITU. ITU-T Fecfhh-rDss (ITU, 2004) (2021). Available: <http://www.itu.int/rec/T-REC-G.97.5.1-200402-I/en> (Accessed December 15, 2021).
46. Aldibbiat NM, Ghassemlooy Z, McLaughlin R. Indoor Optical Wireless Systems Employing Dual Header Pulse Interval Modulation (DH-PIM). *Int J Commun Syst* (2005) 18(3):285-305. doi:10.1002/dac.704

Conflict of Interest: The authors declare that the research was conducted in the absence of any commercial or financial relationships that could be construed as a potential conflict of interest.

Publisher's Note: All claims expressed in this article are solely those of the authors and do not necessarily represent those of their affiliated organizations, or those of the publisher, the editors and the reviewers. Any product that may be evaluated in this article, or claim that may be made by its manufacturer, is not guaranteed or endorsed by the publisher.

Copyright © 2022 Han, Li, Chang, Gao, Zhang, Liao, Wang and Xie. This is an open-access article distributed under the terms of the Creative Commons Attribution License (CC BY). The use, distribution or reproduction in other forums is permitted, provided the original author(s) and the copyright owner(s) are credited and that the original publication in this journal is cited, in accordance with accepted academic practice. No use, distribution or reproduction is permitted which does not comply with these terms.